

File Copy

BRL R 1651

BRL

AD 763/97

REPORT NO. 1651

CALCULATIONS OF TURBULENT SHEAR STRESS IN
SUPERSONIC TURBULENT BOUNDARY LAYER ZERO AND
ADVERSE PRESSURE GRADIENT FLOW

by

Walter B. Sturek

June 1973

Approved for public release; distribution unlimited.

USA BALLISTIC RESEARCH LABORATORIES
ABERDEEN PROVING GROUND, MARYLAND

Destroy this report when it is no longer needed.
Do not return it to the originator.

Secondary distribution of this report by originating
or sponsoring activity is prohibited.

Additional copies of this report may be obtained
from the National Technical Information Service,
U.S. Department of Commerce, Springfield, Virginia
22151.

The findings in this report are not to be construed as
an official Department of the Army position, unless
so designated by other authorized documents.

B A L L I S T I C R E S E A R C H L A B O R A T O R I E S

REPORT NO. 1651

JUNE 1973

CALCULATIONS OF TURBULENT SHEAR STRESS IN SUPERSONIC TURBULENT
BOUNDARY LAYER ZERO AND ADVERSE PRESSURE GRADIENT FLOW

Walter B. Sturek

Exterior Ballistics Laboratory

Approved for public release; distribution unlimited.

RDT&E Project No. 1T061102A33D

A B E R D E E N P R O V I N G G R O U N D , M A R Y L A N D

B A L L I S T I C R E S E A R C H L A B O R A T O R I E S

REPORT NO. 1651

WBSturek/lca
Aberdeen Proving Ground, Md.
June 1973

CALCULATIONS OF TURBULENT SHEAR STRESS IN SUPERSONIC TURBULENT
BOUNDARY LAYER ZERO AND ADVERSE PRESSURE GRADIENT FLOW

ABSTRACT

Calculations of turbulent shear stress distributions are reported for zero pressure gradient and adverse pressure gradient supersonic turbulent boundary layer flow. The calculations are accomplished by numerically integrating the equation for conservation of streamwise momentum using mean profile experimental data. The mixing length distributions have also been determined and indicate that the mixing length distribution is significantly altered for the adverse pressure gradient flow. Finite difference boundary layer computations using an altered mixing length distribution show improved agreement with experimental measurements of skin friction for the adverse pressure gradient flow.

TABLE OF CONTENTS

	Page
ABSTRACT	3
LIST OF ILLUSTRATIONS	7
LIST OF SYMBOLS	9
I. INTRODUCTION	11
II. ANALYSIS OF ZERO PRESSURE GRADIENT DATA	12
A. Shear Stress Profile	12
B. Velocity Derivative	13
C. Eddy Viscosity and Mixing Length	13
D. Analysis of Mixing Length Distribution Anomalous Behavior	13
III. ANALYSIS OF ADVERSE PRESSURE GRADIENT DATA	15
A. Shear Stress Distribution	15
B. Velocity Derivative	17
C. Mixing Length and Eddy Viscosity Profiles	17
IV. NUMERICAL CALCULATION USING MODIFIED MIXING LENGTH DISTRIBUTIONS	17
V. CONCLUSIONS	19
REFERENCES	21
DISTRIBUTION LIST	41

LIST OF ILLUSTRATIONS

Figure		Page
1.	Tunnel Wall Configuration and Test Station Identification .	23
2.	Turbulent Shear Stress Distribution	24
3.	Velocity Derivative Profile, $dp/dx = 0$	25
4.	Calculated Mixing Length Distribution, $dp/dx = 0$	26
5.	Calculated Eddy Viscosity Distribution, $dp/dx = 0$	27
6.	Mixing Length Distributions Obtained Using Different Inputs for the Velocity Derivative	28
7.	Experimental Velocity Profile Compared to the Law of the Wall Correlation	29
8.	Experimental Velocity Derivative Compared to the Result Obtained Using the Law of the Wall Correlation	30
9.	Lines of Constant Mass Flux for Flow Over the Ramp Model .	31
10.	Distribution of the Streamwise Derivative of Mass Flux . .	32
11.	Calculated Shear Stress Profiles for the Flow Over the Ramp Model	33
12.	Turbulent Fluctuation Data Obtained Using Constant Temperature Hot Wire Anemometry	34
13.	Velocity Derivative Profile, $dp/dx > 0$	35
14.	Calculated Mixing Length Distributions, $dp/dx > 0$	36
15.	Calculated Eddy Viscosity Distributions, $dp/dx > 0$	37
16.	Comparison of Experimental Velocity Profile with Finite- Difference Computations	38
17.	Numerical Calculations of Skin Friction Coefficient Compared to Experimental Measurements	39
18.	Comparison of Skin Friction Calculations for Adverse Pressure Gradient Flow Using Unconventional Values for K	40

LIST OF SYMBOLS

A	correction constant, see equation 10
c_f	skin friction coefficient, $2\tau_w/\rho_\infty u_\infty^2$
K	constant in the mixing length relation, $\ell = Ky$
ℓ	mixing length
L	reference length, 2.54 cm
M	Mach number
p	pressure
R	radius of longitudinal curvature
u	streamwise velocity component
u_τ	friction velocity, $(\tau_w/\rho_w)^{1/2}$
v	velocity component normal to the local surface
x	streamwise coordinate
y	coordinate normal to the local surface
β	curvature correction factor, $1/(1+\kappa y)$
γ	ratio of specific heats, c_p/c_v
δ	boundary layer thickness
δ_u	boundary layer velocity thickness
ϵ	turbulent eddy viscosity, see equation 4
θ	boundary layer momentum thickness
κ	inverse longitudinal curvature, $1/R$
μ	molecular viscosity
ρ	density
τ	shear stress

LIST OF SYMBOLS (Continued)

$$\sigma \quad [(\gamma-1)/2] M_{\infty}^2 / [1 + [(\gamma-1)/2] M_{\infty}^2]$$

Subscripts

w property evaluated at the wall

∞ reference condition, property evaluated external to the
 boundary layer for $dp/dx = 0$ and at $y = \delta$ for $dp/dx > 0$

Superscripts

()' turbulent fluctuation component

($\bar{}$) time averaged quantity

I. INTRODUCTION

Since no extensive direct measurements had been reported of the turbulent shear stress distribution in the supersonic turbulent boundary layer until the recent experiment of Rose^{1*}, models of the shear stress distribution have been obtained by extending results found for the more thoroughly measured incompressible turbulent boundary layer. This extension is justified on the basis of available turbulent fluctuation data that indicate little change in the structure of the turbulent fluctuations for the supersonic ($M = 1.2-5.0$) turbulent boundary layer compared to that obtained in the incompressible turbulent boundary layer for zero pressure gradient, adiabatic flow. Furthermore, calculations were reported by Maise and McDonald² for zero pressure gradient, adiabatic flow in which the shear stress, eddy viscosity and mixing length distributions were determined by a finite difference solution of the boundary layer equations using a "law of the wall" velocity correlation. These calculations revealed that the mixing length distribution was essentially unchanged as the Mach number ranged from zero to five. The eddy viscosity distribution, however, was shown to exhibit a sensitivity to both Reynolds number and Mach number.

Calculation procedures employing a shear stress distribution established from incompressible turbulent boundary layer characteristics have, in general, yielded good agreement with experimental data for the supersonic turbulent boundary layer zero pressure gradient or mildly favorable pressure gradient, adiabatic flow. Less satisfactory results are obtained when computing flow in which adverse pressure gradient and longitudinal curvature are encountered^{4,5,6,7}. One obvious source for error is the inability of present computational procedures to properly account for the pressure gradient normal to the surface. Another source of uncertainty lies in the behavior of the distribution of turbulent shear stress. Although turbulent fluctuation data indicate similar behavior for incompressible and supersonic zero pressure gradient turbulent boundary layers, distinct differences are apparent in the profiles of turbulent fluctuations between supersonic zero pressure gradient and supersonic adverse pressure gradient turbulent boundary layer flow^{8,9,14}.

This report describes calculations of turbulent shear stress, mixing length and eddy viscosity distributions using the mean profile data reported in reference 9. These data were obtained in a Mach 3.5 nozzle wall turbulent boundary layer for zero pressure gradient and an isentropic-ramp-induced adverse pressure gradient flow (see Figure 1). The method for calculating the shear stress distribution for the zero pressure gradient data is similar to that of Meier and Rotta¹⁰. The procedure for calculating the shear stress profile for the flow over the ramp model was developed from the boundary layer equations applicable to compressible flow over a surface with longitudinal curvature.

* References are listed on page 21.

A similar procedure applied to experimental data for this flow configuration has not been previously reported.

II. ANALYSIS OF ZERO PRESSURE GRADIENT DATA

A. Shear Stress Profile

The equations for conservation of mass and conservation of stream-wise momentum applicable to zero pressure gradient, adiabatic compressible flow over a flat plate can be combined and integrated in the direction normal to the surface to yield

$$\int_0^y \frac{\partial}{\partial x} (\rho u^2) dy - u \int_0^y \frac{\partial}{\partial x} (\rho u) dy = \tau - \tau_w \quad (1)$$

Assuming the flow to be locally similar enables equation (1) to be written in dimensionless form as

$$\frac{1}{\rho_\infty u_\infty^2} (\tau - \tau_w) = \frac{1}{\delta} \frac{d\delta}{dx} \left[\int_0^y \left(\frac{\rho u^2}{\rho_\infty u_\infty^2} \right) dy - \frac{u}{u_\infty} \int_0^y \frac{\rho u}{\rho_\infty u_\infty^2} dy \right] \quad (2)$$

The assumption of "locally similar flow" (see references 3, 10 and 11) is not expected to be fully satisfied. However, in the vicinity near the wall where the assumption of similarity is poorest, the contribution of the convective terms is minimal. The equality $(1/\delta)(d\delta/dx) = (1/\theta)(d\theta/dx)$ also follows from similarity. Introducing this equality and the relation $(d\theta/dx = c_f/2)$ into equation (2) yields after rearranging

$$\frac{\tau}{\tau_w} = 1 + \frac{1}{2\theta \rho_\infty u_\infty^2} \left[\int_0^y \rho u dy - u \int_0^y \rho u dy \right] \quad (3)$$

The integrals in equation (3) were evaluated numerically using the tabulated profile data of reference 9. The numerical integration was carried out using the standard Fortran subroutine AVINT which fits a parabola to the data. An example of the profile obtained is shown in Figure 2 compared to that obtained by Maise and McDonald². These profiles are in reasonable agreement except near the edge of the boundary layer. The profile from reference 2 goes to zero at $y/\delta = 1$ with a finite slope whereas the profile calculated here approaches zero asymptotically beyond the edge of the boundary layer. This behavior is consistent with the profile of turbulent fluctuations as measured using hot-wire anemometry (see references 8, 9 and 12).

B. Velocity Derivative

Also needed for the calculation of eddy viscosity or mixing length distributions is the distribution of the velocity derivative, du/dy . This was calculated from the experimental data using a central difference technique. An example of the profiles obtained is shown in Figure 3. No attempt was made to smooth the data since it was felt that the scatter indicated by the data would, in itself, be of interest in revealing the uncertainty in the eddy viscosity and mixing length distributions obtained. The viscous sublayer is extremely thin

($y^+ = 10 \rightarrow y \approx .004$ -inch) for the experimental data considered here. The value of $d(u/u_\infty)/d(y/\delta)$ corresponding to the measured wall shear stress is approximately 90.

C. Eddy Viscosity and Mixing Length

The eddy viscosity and mixing length distributions were calculated using the relations

$$\frac{\epsilon}{u_\infty \delta u} = \frac{1}{u_\infty \delta u} \left[\frac{\tau}{\rho \frac{du}{dy}} \right] \quad (4)$$

$$\frac{\ell}{\delta} = \frac{1}{\delta} \left[\frac{\tau}{\rho (du/dy)^2} \right]^{1/2} \quad (5)$$

where the local value of density was obtained from the tabulated profile data.

An example of the mixing length distribution obtained is shown in Figure 4. The data in the wall region of the boundary layer agree very well with the accepted relation $\ell = .4y$. The magnitude in the region of the plateau (about 0.055) is considerably less than the generally accepted value of 0.089. The trend of ℓ/δ increasing for $y/\delta > .6$ has been observed in other calculations³ and will be discussed further in the next section.

An example of the eddy viscosity distribution obtained is shown in Figure 5 compared to profiles from reference 2. The peak value is significantly less than that in reference 2. The trend of the profile for $y/\delta > .6$ again deviates from the trend of the profiles of reference 1.

D. Analysis of Mixing Length Distribution Anomalous Behavior

There are two trends shown in the mixing length distribution that invite question: (1) the low value of the plateau region, and (2) the behavior for $y/\delta > 0.6$. The cause for the seemingly anomalous behavior

was sought by comparing the results obtained when the shear stress distribution calculated here was replaced by that of reference 2, and likewise, for the distribution of the velocity derivative, du/dy .

The mixing length distribution obtained using the shear stress profile of reference 2 was virtually identical to that in Figure 4. The next step taken was to alternate profiles of the velocity derivative. The velocity profile used in reference 2 was a compressible "law of the wall" correlation. Equation 11 of reference 2, which was obtained by inverting the velocity defect correlation is repeated below.

$$\frac{u}{u_{\infty}} = \frac{1}{\sqrt{\sigma}} \sin \left\{ - \frac{u_{\tau}}{u_{\infty}} \sqrt{\sigma} \left[2.5 \log_e \left(\frac{y}{\delta} \right) + 1.25 \left[1 + \cos \frac{\pi y}{\delta} \right] + \arcsin \sqrt{\sigma} \right] \right\} \quad (6)$$

where

$$\sigma = \frac{[(\gamma-1)/2] M_{\infty}^2}{1 + [(\gamma-1)/2] M_{\infty}^2}$$

This expression was differentiated to yield the velocity derivative in the y direction. The constant 1.25 in equation (6) is the ratio, Π/K , where Π is Coles' wake parameter and K is the constant in the relation $\ell = Ky$. Using the calculated velocity derivative, the density profile from the tabulated data, and both the shear stress profile calculated here and that from reference 2, the value of ℓ/δ in the plateau region was about 0.11.

Since a value of Π/K of 2.25 was found to correlate the experimental data of reference 9, this value was substituted into equation (6). The mixing length distribution now obtained is shown in Figure 6 for the two shear stress distributions. The value of ℓ/δ in the plateau region is about 0.070. The trend for ℓ/δ to increase for $y/\delta > 0.6$ is obviously the effect of the calculated shear stress profile approaching zero asymptotically beyond $y/\delta = 1.0$.

In comparing the velocity distribution calculated using equation (6) for $\Pi/K = 2.25$ with the experimental data, a significant disagreement is noted in the region for $y/\delta < 0.4$. This is shown in Figure 7. The effect of this discrepancy on the velocity derivative is shown in Figure 8. The region of significant disagreement lies between $y/\delta = 0.15$ and $y/\delta = 0.6$. This is the region in which the plateau forms as noted in Figure 4. Although the data correlate in velocity defect coordinates, this type of correlation is not sufficiently accurate to extract a valid profile for the velocity derivative.

The conclusions reached regarding the mixing length distribution are: (1) the profile of Figure 4 is a valid representation of the effective mixing length for the experimental data considered; and (2) a "law of the wall" velocity correlation is not a sufficiently accurate representation of the velocity profile to enable a valid velocity derivative to be obtained.

III. ANALYSIS OF ADVERSE PRESSURE GRADIENT DATA

A. Shear Stress Distribution

The equations for conservation of mass and streamwise momentum as applicable to two-dimensional, compressible turbulent boundary layer flow over a surface with longitudinal curvature may be expressed as follows.

$$\frac{\partial}{\partial x} (\rho u) + \frac{\partial}{\partial y} [(1 + \kappa y)(\rho v + \overline{\rho'v'})] = 0 \quad (7)$$

$$\begin{aligned} \frac{1}{1+\kappa y} \rho u \frac{\partial u}{\partial x} + (\rho v + \overline{\rho'v'}) \frac{\partial u}{\partial y} + (\rho v + \overline{\rho'v'}) u \frac{\kappa}{1+\kappa y} = \\ - \frac{1}{1+\kappa y} \frac{\partial p}{\partial x} + \frac{\partial}{\partial y} \left[\mu \frac{\partial u}{\partial y} - \rho \overline{u'v'} \right] \end{aligned} \quad (8)$$

These relations result from order of magnitude considerations applied to the more general relations derived by Tetervin¹³.

Equations (7) and (8) may be integrated in the y direction normal to the local surface and combined to yield the following relation for the shear stress distribution.

$$\begin{aligned} \frac{\tau}{\tau_w} = \frac{1}{\tau_w} \left\{ \tau_w + \int_0^y \beta \frac{\partial}{\partial x} (\rho u^2) dy - \right. \\ \left. u\beta \int_0^y \frac{\partial}{\partial x} (\rho u) dy - 2 \int_0^y \left[\int_0^y \frac{\partial}{\partial x} (\rho u) dy \right] u\beta^2 \kappa dy + \right. \\ \left. \int_0^y \beta \frac{\partial p}{\partial x} dy \right\} \end{aligned} \quad (9)$$

where $\beta = \frac{1}{1+\kappa y}$ and $\tau = \mu \frac{\partial u}{\partial y} - \rho u \sqrt{V}$.

This relation has been evaluated directly using measured values of wall shear stress and the tabulated profile data of reference 9. Values of the partial derivatives have been determined along lines of constant mass flux using a least squares technique which fits a parabola to the data. The lines of constant mass flux are shown in Figure 9 along with the change in boundary layer thickness. It is interesting to note that although the boundary layer becomes less thick at downstream stations mass continues to be entrained within the boundary layer. An example of the distribution of the partial derivative $\partial(\rho u)/\partial x$ is shown in Figure 10. In evaluating the shear stress distribution, equation (9) was integrated numerically as discussed previously.

Initial efforts to calculate the shear stress distribution resulted in profiles with a large (about $6 \tau_w$) negative value in the vicinity of the boundary layer outer edge. After examining the accuracy of the profiles of the partial derivatives, it was concluded that these partial derivatives could be in error by as much as ± 30 percent. In order to obtain physically meaningful profiles for the shear stress distribution, the partial derivative of mass flux, $\partial(\rho u)/\partial x$, was corrected as indicated below. The corrected profile is also shown in Figure 10.

$$\frac{\partial}{\partial x} (\rho u)_{\text{corrected}} = \frac{\partial}{\partial x} (\rho u) [A + (1-A)(y/\delta)] \quad (10)$$

$$0 \leq (y/\delta) \leq 1$$

$$\frac{\partial}{\partial x} (\rho u)_{\text{corrected}} = \frac{\partial}{\partial x} (\rho u) \quad y > 1.0 \quad (11)$$

A computation iteration loop was used to determine the value of the constant A that resulted in the shear stress profile remaining greater than zero throughout the boundary layer. The value of A varied from station to station and ranged between 0.7750 at the first station and 0.6875 at the last station on the ramp model. The shear stress profiles obtained are shown in Figure 11. These profiles are consistent with the boundary condition at the wall, $d\tau/dy = dp/dx$, and with the trend of the fluctuation data shown in Figure 12. The turbulent fluctuation data were obtained using constant temperature hot wire anemometry. These data are plotted as an arbitrary dimensionless number determined by dividing the measured signal by 0.005 volt. Returning to Figure 11, the trend of the shear stress profile to increase beyond the point of minimum shear stress is inconsistent with the requirement that τ approach zero in the vicinity of the edge of the boundary layer. This trend is believed to be a result of the uncertainty in determining the streamwise partial derivatives.

A check was made to assess the effect on the shear stress profiles of adjusting the partial derivative $\partial(\rho u^2)/\partial x$ and comparing the results with those obtained by correcting $\partial(\rho u)/\partial x$. The profiles were in close agreement both in trend and magnitude.

B. Velocity Derivative

The velocity derivative, du/dy , was calculated directly from the tabulated profile data in the same manner as discussed previously. An example of the velocity derivative for the flow over the ramp model is given in Figure 13. This profile is significantly unlike that of Figure 3 in the wake portion of the boundary layer. The greater value of du/dy in this portion of the boundary layer is consistent with the trend of the fluctuation data since $(\overline{u'}^2)$ can be considered to be proportional to $(du/dy)^2$.

C. Mixing Length and Eddy Viscosity Profiles

The distributions of mixing length and eddy viscosity were calculated using equations (4) and (5) as discussed previously.

An example of the mixing length profiles obtained is shown in Figure 14. These profiles are considerably distorted compared to that obtained in the region of zero pressure gradient. The first characteristic of interest is the change in value of K in the relation $\ell = Ky$. A value for K of 0.65 appears to fit the data points in the vicinity of the wall. A second characteristic of interest is the increase in peak value at succeeding downstream stations. The behavior of the mixing length profiles for $y/\delta > 0.5$ is suspect due to the uncertainty associated with the calculated shear stress profiles.

The distribution of eddy viscosity is shown in Figure 15. These profiles are similar to the profiles obtained for zero pressure gradient flow with the following exceptions: (1) the peak value changes at different streamwise positions; and (2) the magnitude of the peak value is from 2 to 4.5 times the value obtained for the zero pressure gradient flow.

IV. NUMERICAL CALCULATION USING MODIFIED MIXING LENGTH DISTRIBUTIONS

The boundary layer properties have been calculated using the computer program of Hixon, Beckwith and Bushnell¹⁵. This program is an implicit finite-difference procedure that calculates turbulent flow using an eddy viscosity model based on a mixing length distribution. The mixing length distribution is modified for the effect of wall damping in a very small region close to the wall by using Van Driest's exponential damping function. Calculations have been run using the conventional mixing length distribution as well as those calculated here.

The conventional mixing length distribution used was:

$$\begin{aligned} \ell/\delta &= 0.4 y/\delta & \text{for} & \quad y/\delta \leq 0.1 \\ \ell/\delta &= 0.04 + \left[\frac{(y/\delta) - 0.1}{.2} \right] (.06) & \text{for} & \quad 0.1 < y/\delta \leq 0.3 \quad (12) \\ \ell/\delta &= 0.10 & \text{for} & \quad y/\delta > 0.3 \end{aligned}$$

Other mixing length distributions used were:

(1) zero pressure gradient

$$\begin{aligned} \ell/\delta &= 0.4 y/\delta & \text{for} & \quad y/\delta \leq 0.1 \\ \ell/\delta &= 0.04 + \left[\frac{(y/\delta) - 0.1}{.2} \right] (.015) & \text{for} & \quad 0.1 < y/\delta \leq 0.3 \quad (13) \\ \ell/\delta &= .055 & \text{for} & \quad 0.3 < y/\delta < 0.65 \\ \ell/\delta &= .1857 (y/\delta - .65) + .055 & \text{for} & \quad 0.65 \leq y/\delta \leq 1 \\ \ell/\delta &= .12 & \text{for} & \quad y/\delta > 1 . \end{aligned}$$

(2) adverse pressure gradient

$$\begin{aligned} \text{(a)} \quad \ell/\delta &= 0.65 y/\delta & \text{for} & \quad y/\delta \leq 0.1 \\ \ell/\delta &= 0.065 + \left[\frac{(y/\delta) - 0.1}{.2} \right] (.035) & \text{for} & \quad 0.1 < y/\delta \leq 0.3 \quad (14) \\ \ell/\delta &= .08 & \text{for} & \quad y/\delta > 0.3 \\ \text{(b)} \quad \ell/\delta &= 0.5 y/\delta & \text{for} & \quad y/\delta \leq 0.1 \\ \ell/\delta &= 0.05 + \left[\frac{(y/\delta) - 0.1}{.2} \right] (.05) & \text{for} & \quad 0.1 < y/\delta \leq 0.3 \quad (15) \\ \ell/\delta &= .08 & \text{for} & \quad y/\delta > 0.3 \end{aligned}$$

The calculations were started using measured profiles of velocity and total temperature. The program then calculates the density profile assuming constant static pressure across the boundary layer. The effective length or starting point for the boundary layer development has been taken as the nozzle throat for the calculations shown here.

Velocity profiles for the zero pressure gradient flow calculated using the mixing length distributions given as equations (12) and (13) are shown in Figure 16 compared to the experimental data. The calculations using the conventional mixing length distribution predict a velocity profile that is too full compared to the measured profile; however, the calculations using the mixing length distribution determined here (equation 13) show very good agreement with the experimental data. It cannot be concluded that these results are true for the compressible turbulent boundary layer in general. However, the response of the numerical program to the calculated mixing length distribution does indicate that equation (13) is a valid representation of the effective mixing length distribution for the experimental data considered.

Calculated results for skin friction coefficient are shown in Figure 17 compared to experimental measurements of skin friction coefficient. The conventional mixing length distribution yields good agreement with the experimental data for zero pressure gradient flow. The agreement for the calculated mixing length distribution is also within the accuracy of the experimental data. As the calculation proceeds downstream, the skin friction coefficient begins to decrease when the flow encounters the adverse pressure gradient. Values for skin friction coefficient calculated using the conventional mixing length distribution are 15-20% low compared to the experimentally measured values for the adverse pressure gradient flow.

Additional calculations for the adverse pressure gradient flow are shown in Figure 18. These calculations were started at the first test station on the ramp model using measured profiles of velocity and total temperature. Again, the calculated values of skin friction coefficient are about 20% low compared to the experimental measurements when the conventional mixing length distribution is used. The calculations using a value for K of 0.65 yield values of skin friction coefficient that are about 40% too great. However, the calculations run using a value for K of 0.50 do show promise. These results agree within $\pm 5\%$ of the measured values.

V. CONCLUSIONS

Calculations have been made of the turbulent shear stress distribution for compressible zero pressure gradient and adverse pressure gradient boundary layer flow. The effective mixing length and eddy viscosity distributions have been determined using these calculated distributions of turbulent shear stress.

In order to obtain physically meaningful distributions of turbulent shear stress for the adverse pressure gradient flow, it was necessary to adjust the profile for the partial derivative, $\frac{\partial}{\partial x}(\rho u)$, that was determined directly from the tabulated profile data. It is recognized that the resulting shear stress profiles invite some uncertainty due to this procedure. However, it is felt that the calculations reported are physically meaningful and that the results indicate trends which could lead to improved prediction of compressible turbulent boundary layer development in an adverse pressure gradient.

The conclusions reached on the results of this investigation are summarized below.

(1) The mixing length distribution shown in Figure 4 is a valid representation of the effective mixing length distribution for the zero pressure gradient data considered.

(2) The value of the constant K in the relation $\ell = Ky$ changed from 0.4 for zero pressure gradient flow to 0.65 for the adverse pressure gradient flow.

(3) The maximum values of τ/τ_w increased as the flow proceeded in the streamwise direction in the region of adverse pressure gradient. This increase in $(\tau/\tau_w)_{\max}$ resulted in the value of $(\ell/\delta)_{\max}$ likewise increasing at downstream stations in the adverse pressure gradient.

(4) Both the conventional and the calculated mixing length distributions yielded good agreement with experimental measurements of wall shear stress for zero pressure gradient flow when used in a finite difference boundary layer computer program.

(5) The best agreement of the numerical calculations with experimental measurements of wall shear stress for the adverse pressure gradient flow was obtained by substituting $K = 0.5$ in the mixing length distribution.

Since the computer program used for these numerical calculations is restricted to a constant static pressure through the boundary layer, it would be of interest to perform calculations of the flow over the ramp model using a program that accounts for the pressure gradient normal to the surface.

REFERENCES

1. William C. Rose, "The Behavior of a Compressible Turbulent Boundary-Layer in a Shock-Wave-Induced Adverse Pressure Gradient," PhD dissertation, University of Washington, 1972.
2. George Maise and Henry McDonald, "Mixing Length and Kinematic Eddy Viscosity in a Compressible Boundary Layer," *AIAA Journal*, Vol. 6, No. 1, January 1968, pp. 73-80.
3. Dennis M. Bushnell and Dana J. Morris, "Shear-Stress, Eddy-Viscosity, and Mixing Length Distributions in Hypersonic Turbulent Boundary Layers," NASA-TM-X-2310, August 1971.
4. H. James Herring and George L. Mellor, "A Method of Calculating Compressible Turbulent Boundary Layers," NASA-CR-1144, September 1968.
5. Larry L. Lynes, Jack N. Nielsen, and Gary D. Kuhn, "Calculation of Compressible Turbulent Boundary Layers with Pressure Gradients and Heat Transfer," NASA-CR-1303, March 1969.
6. Irwin E. Alber and Douglas E. Coats, "Analytical Investigations of Equilibrium and Nonequilibrium Compressible Turbulent Boundary Layers," AIAA Paper No. 69-689, June 1969.
7. T. Cebeci, A. M. O. Smith, and G. Mosinskis, "Calculation of Compressible Adiabatic Turbulent Boundary Layers," AIAA Paper No. 69-687, June 1969.
8. W. B. Sturek and J. E. Danberg, "Supersonic Turbulent Boundary Layer in Adverse Pressure Gradient. Part I: The Experiment," *AIAA Journal*, Vol. 10, No. 4, April 1972, pp. 475-480.
9. W. B. Sturek, "An Experimental Investigation of the Supersonic Turbulent Boundary Layer in a Moderate Adverse Pressure Gradient. Part I. A Detailed Description of the Experiment and Data Tabulation," BRL Report 1506, U.S. Army Ballistic Research Laboratories, Aberdeen Proving Ground, Maryland, October 1970. AD 716336.
10. H. U. Meier and J. C. Rotta, "Experimental and Theoretical Investigations of Temperature Distributions in Supersonic Boundary Layers," AIAA Paper No. 70-744, June 1970.
11. R. L. Simpson, "Characteristics of Turbulent Boundary Layers at Low Reynolds Numbers With and Without Transpiration," *Journal of Fluid Mechanics*, Vol. 42, Part 2, 30 July 1970, p. 787.

12. A. L. Kistler, "Fluctuation Measurements in Supersonic Turbulent Boundary Layers," BRL Report 1052, U.S. Army Ballistic Research Laboratories, Aberdeen Proving Ground, Maryland, August 1958. AD 211278.
13. Neal Tetervin, "An Exploratory Theoretical Investigation of the Effect of Longitudinal Surface Curvature on the Turbulent Boundary Layer," NOL TR-69-22, U.S. Naval Ordnance Laboratory, White Oak, Maryland, February 1969.
14. P. J. Waltrup and J. A. Schetz, "An Experimental Investigation of a Supersonic Turbulent Boundary Layer Subjected to a Systematic Variation of Adverse Pressure Gradients," AIAA Paper No. 72-311, April 1972.
15. B. A. Hixon, Ivan E. Beckwith and D. M. Bushnell, "Computer Program for Compressible Laminar or Turbulent Nonsimilar Boundary Layers," NASA-TM-X-2140, April 1971.

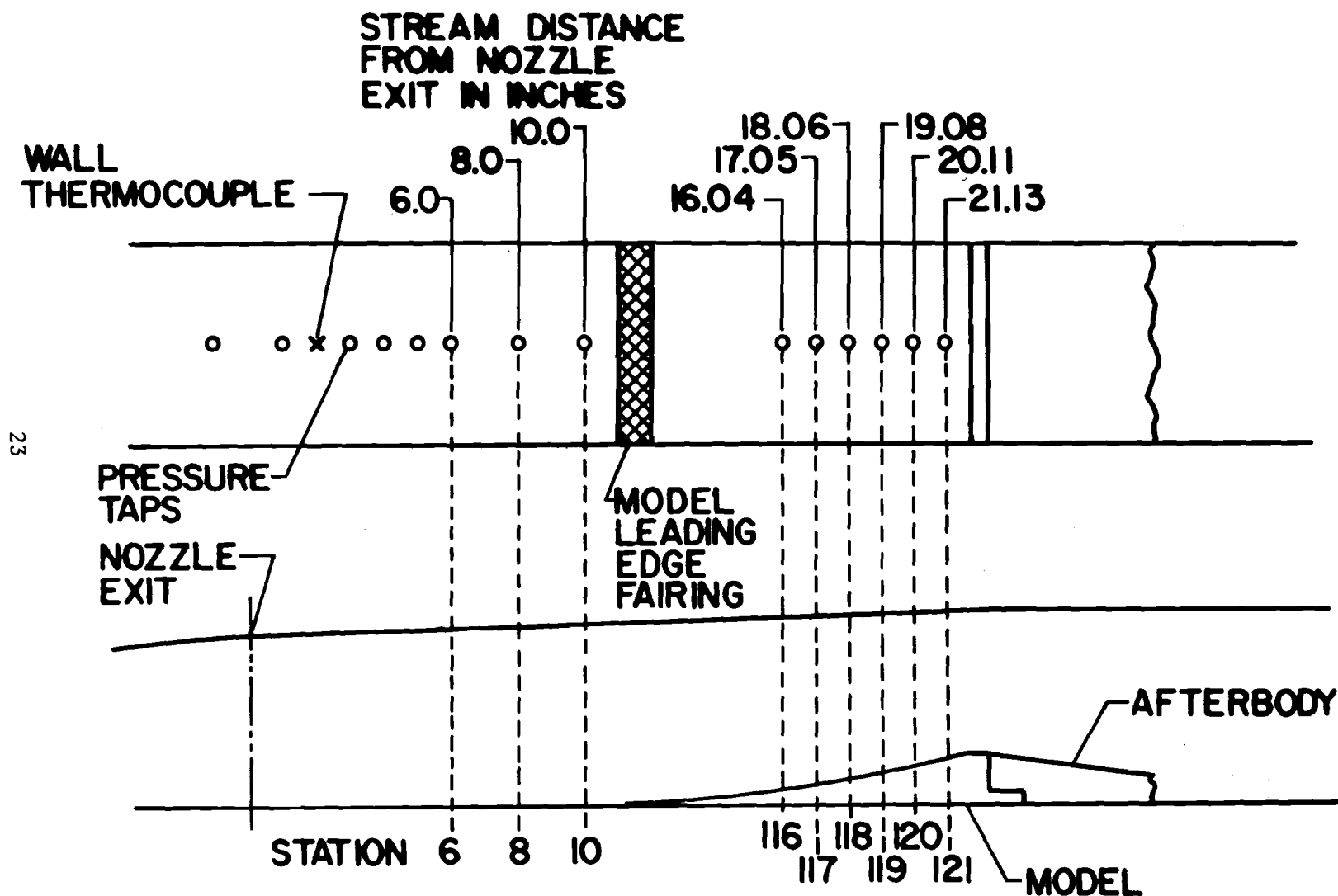


Figure 1. Tunnel Wall Configuration and Test Station Identification

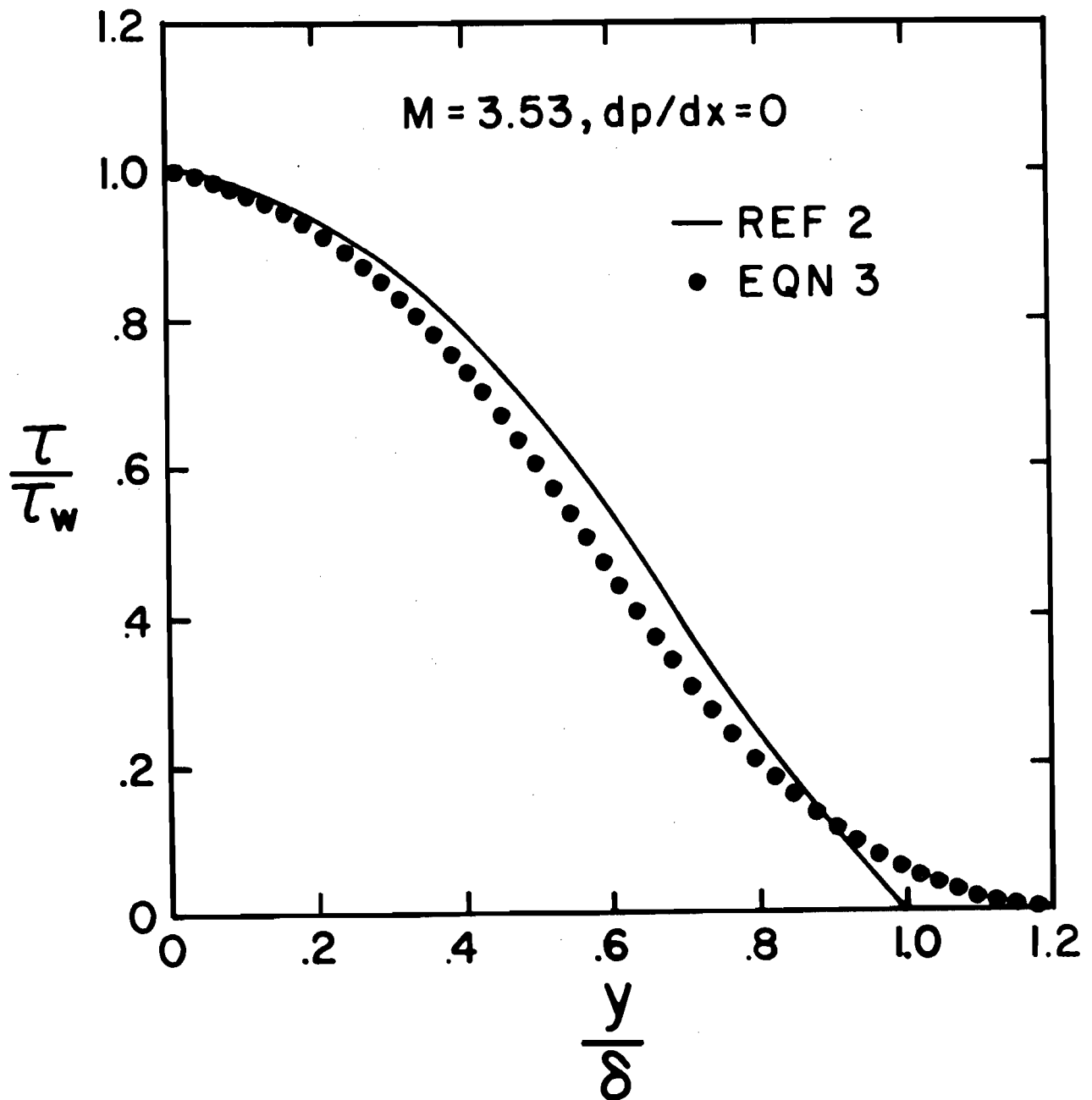


Figure 2. Turbulent Shear Stress Distribution

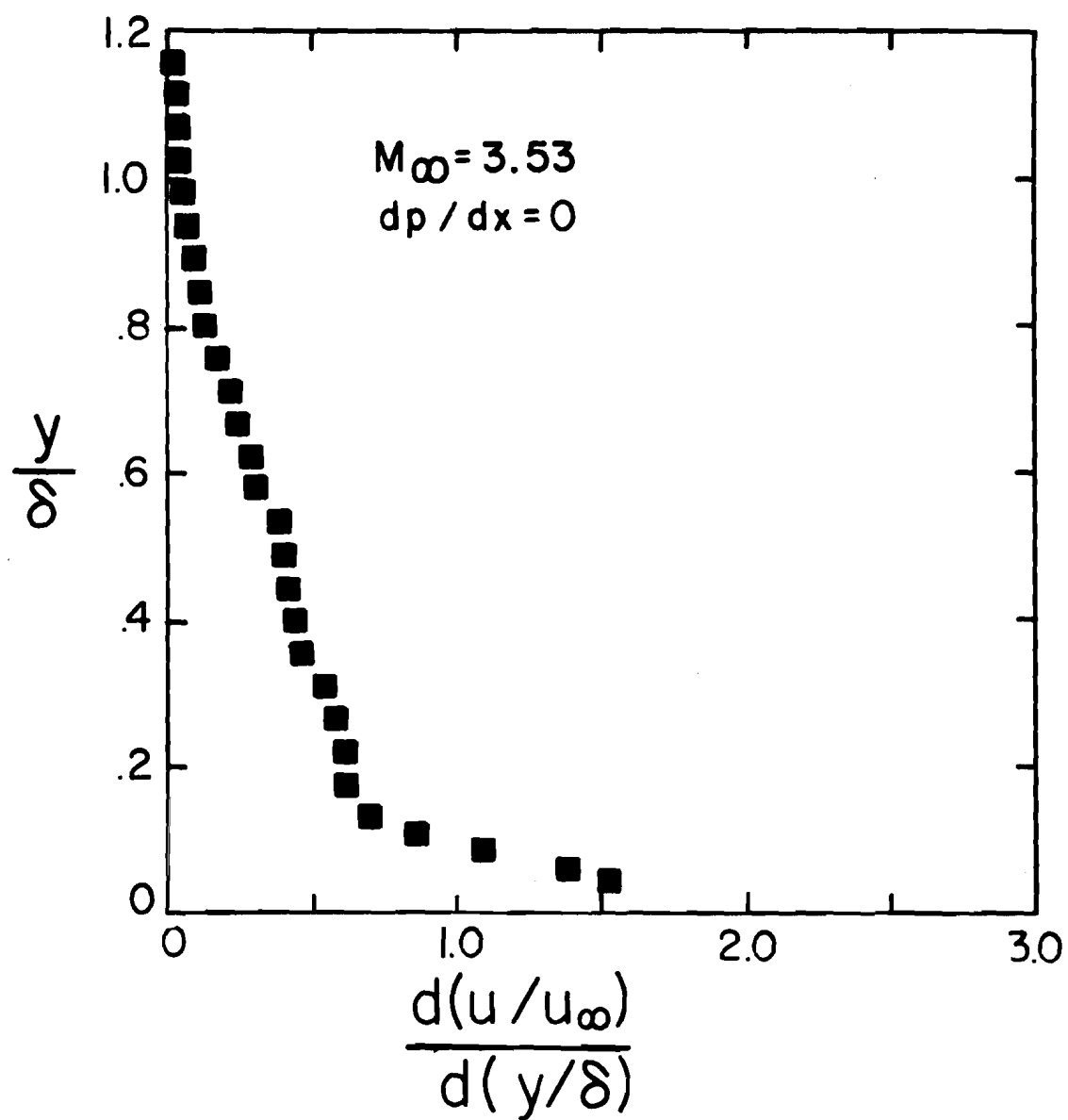


Figure 3. Velocity Derivative Profile, $dp/dx = 0$

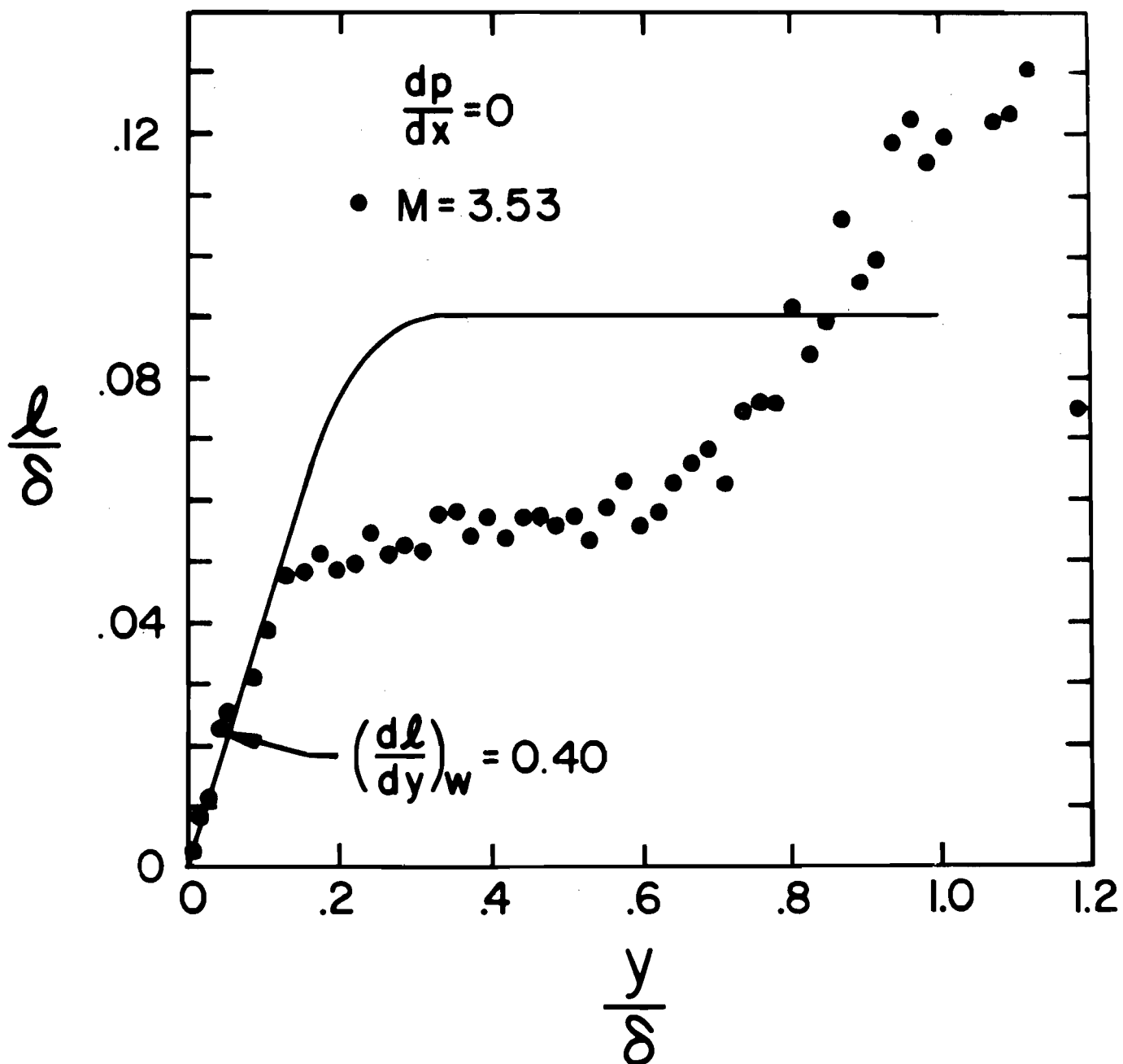


Figure 4. Calculated Mixing Length Distribution, $dp/dx = 0$

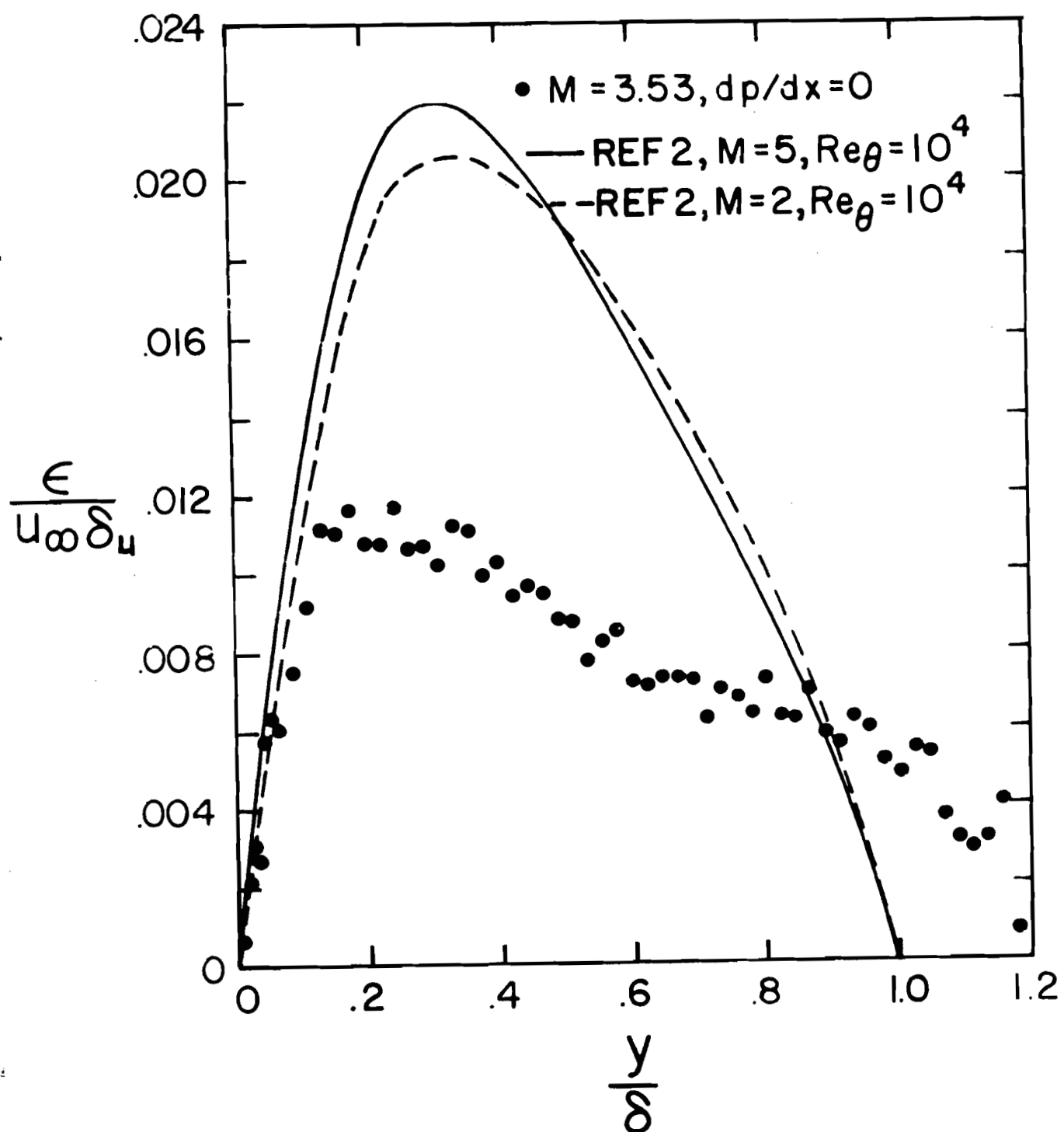


Figure 5. Calculated Eddy Viscosity Distribution, $dp/dx = 0$

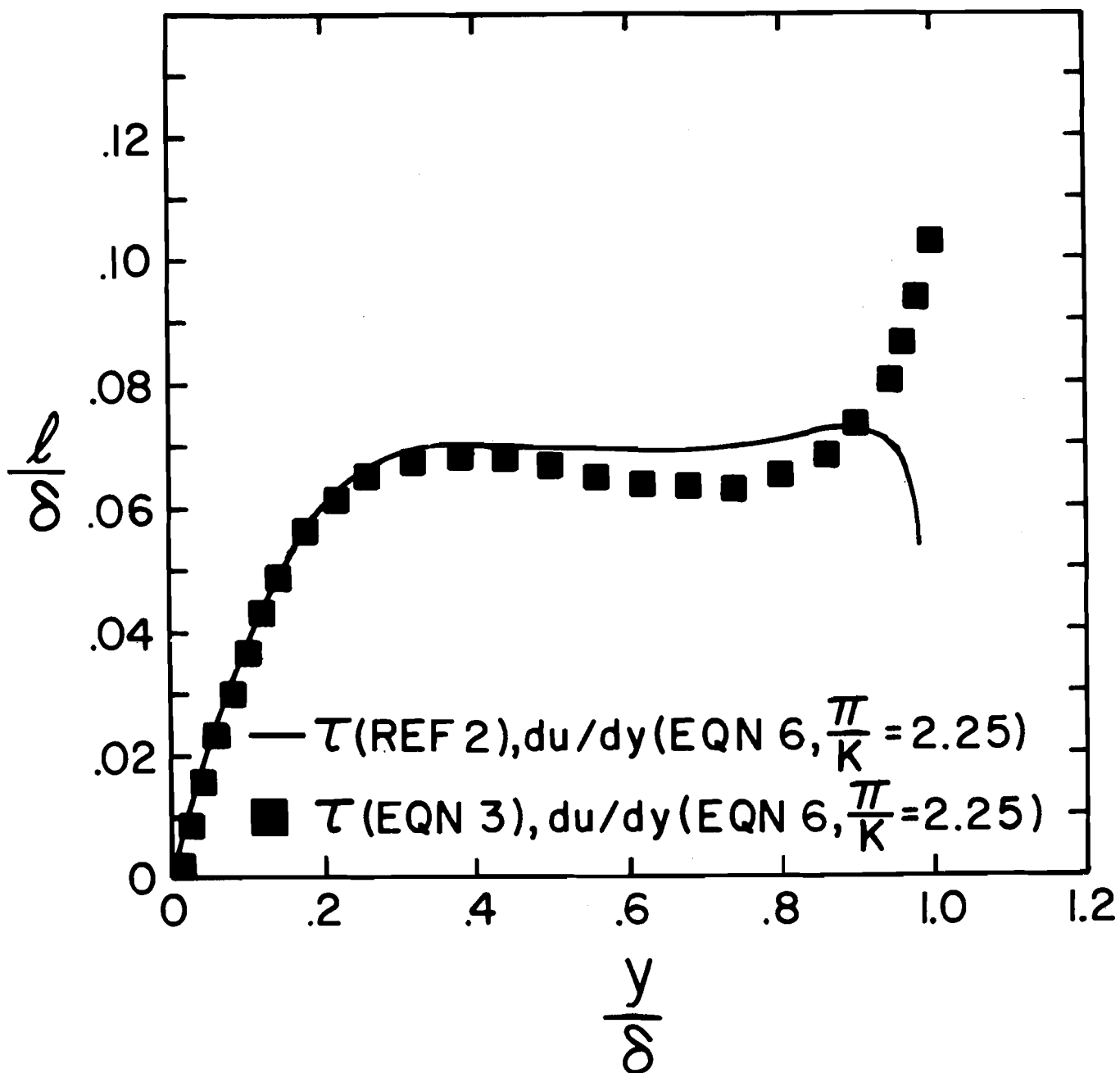


Figure 6. Mixing Length Distributions Obtained Using Different Inputs for the Velocity Derivative

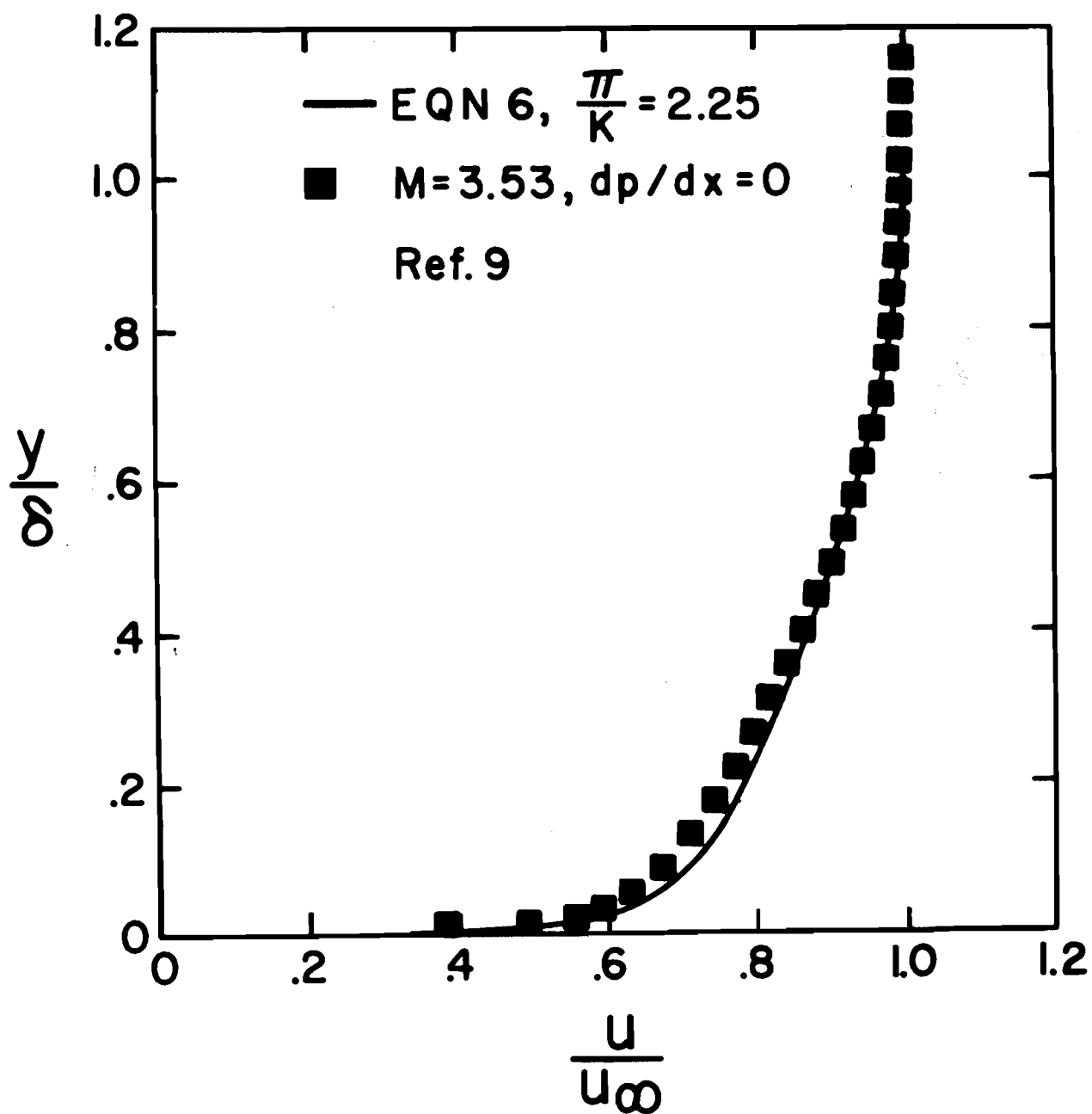


Figure 7. Experimental Velocity Profile Compared to the Law of the Wall Correlation

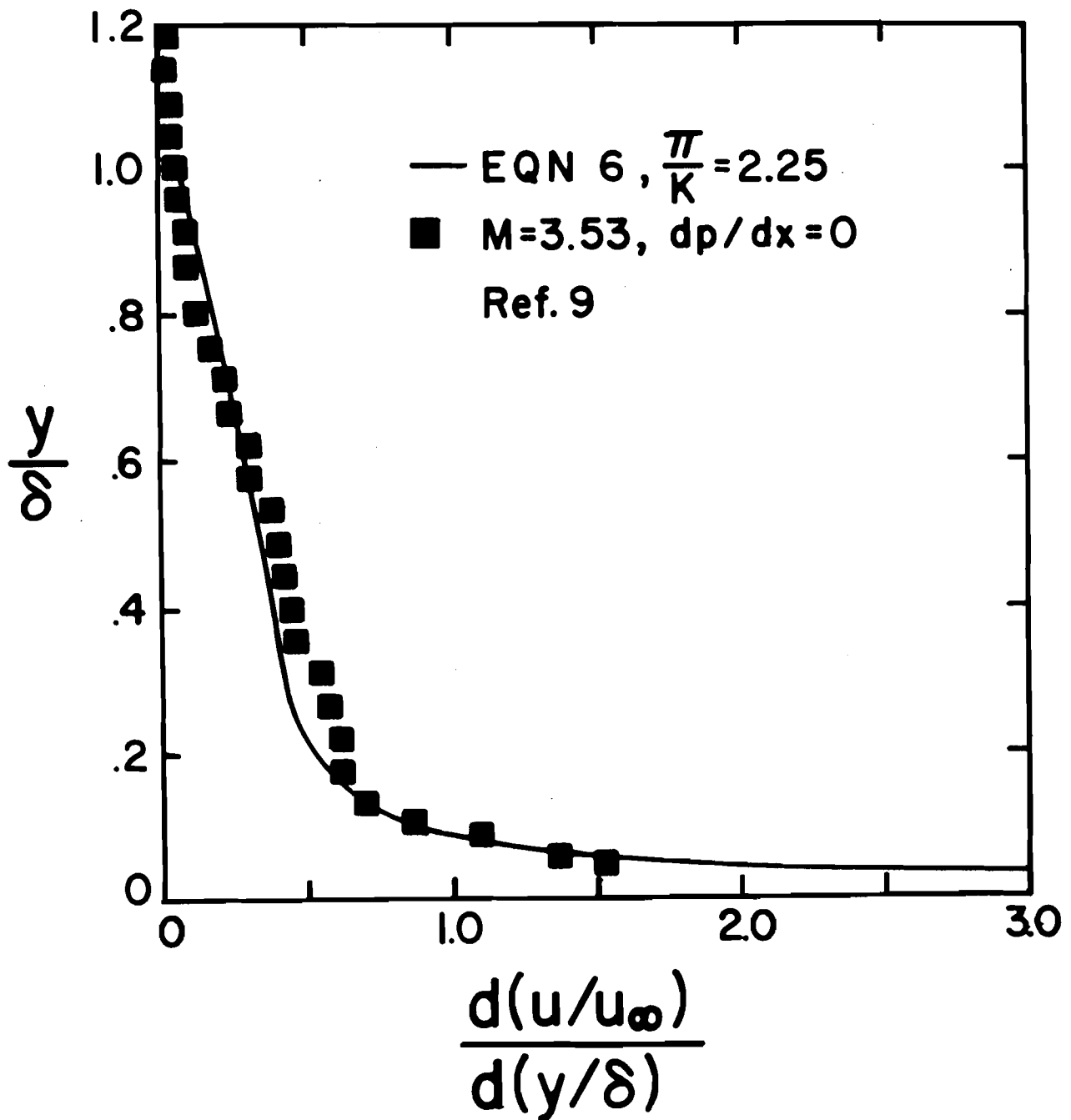


Figure 8. Experimental Velocity Derivative Compared to the Result Obtained Using the Law of the Wall Correlation

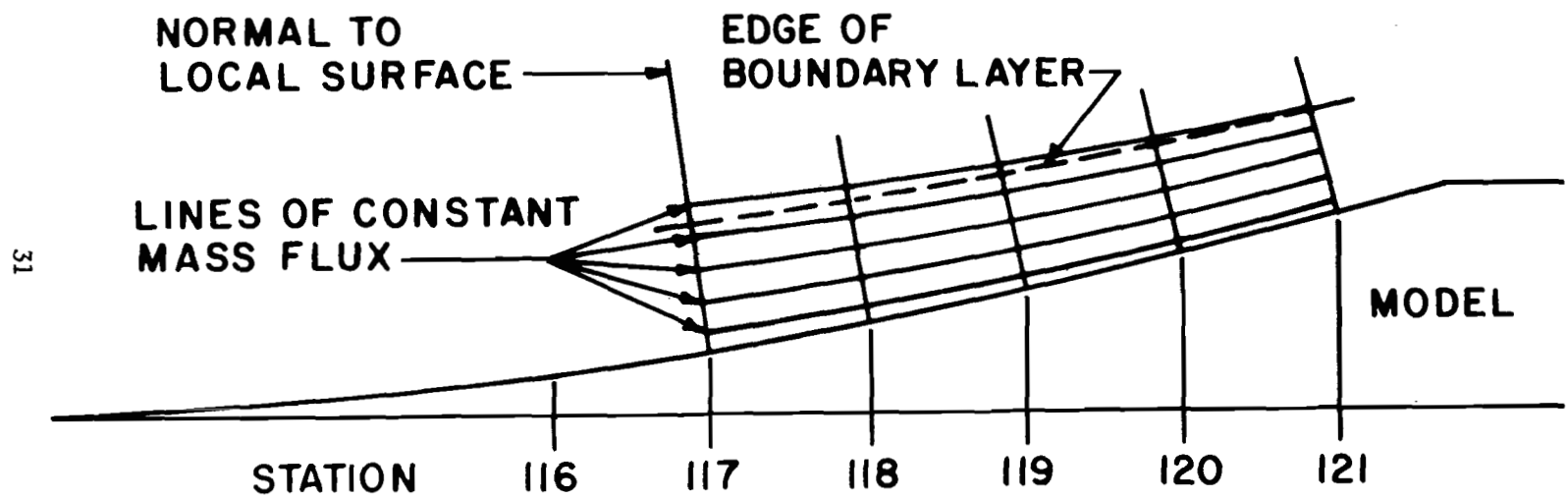


Figure 9. Lines of Constant Mass Flux for Flow Over the Ramp Model

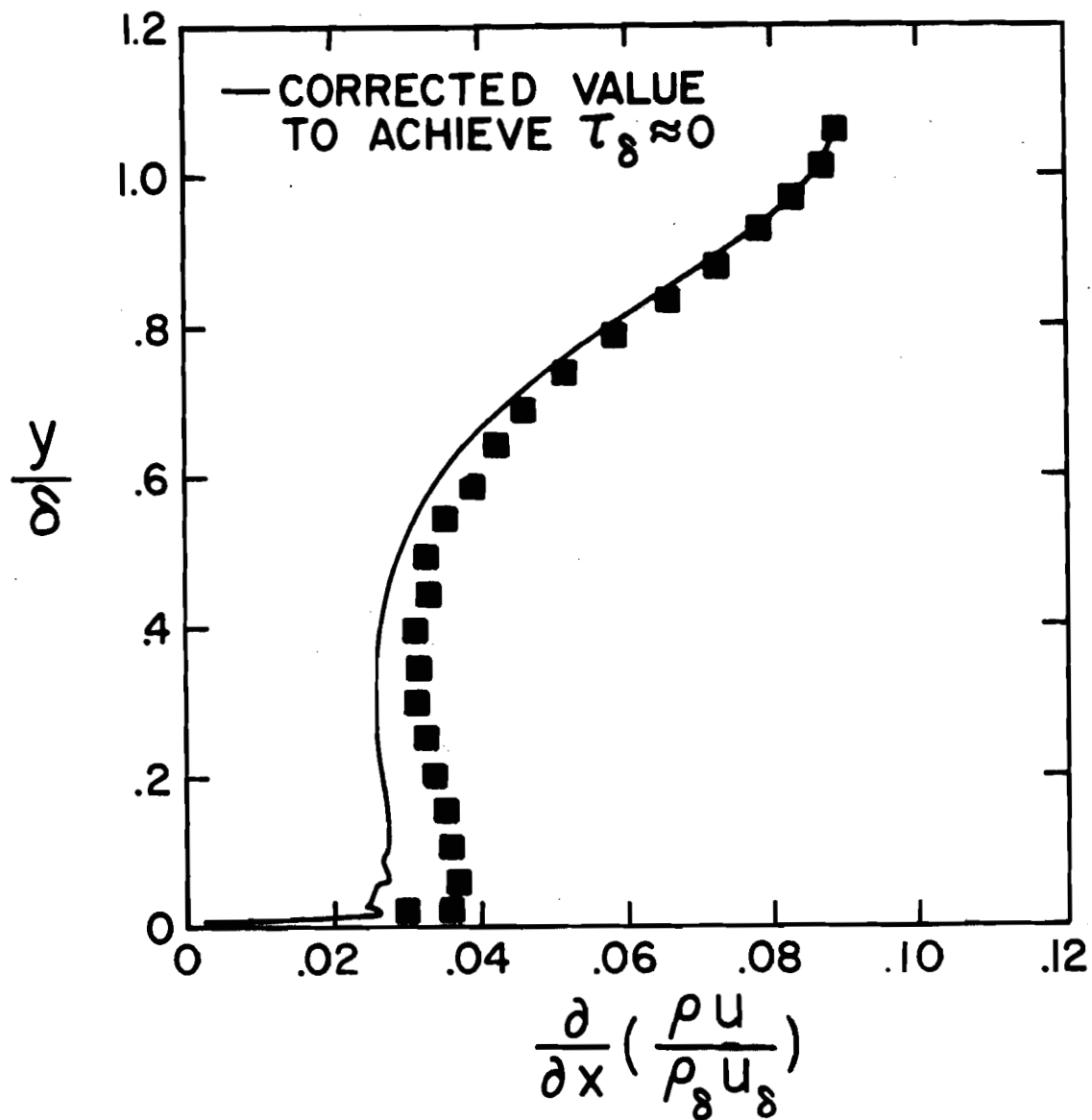


Figure 10. Distribution of the Streamwise Derivative of Mass Flux

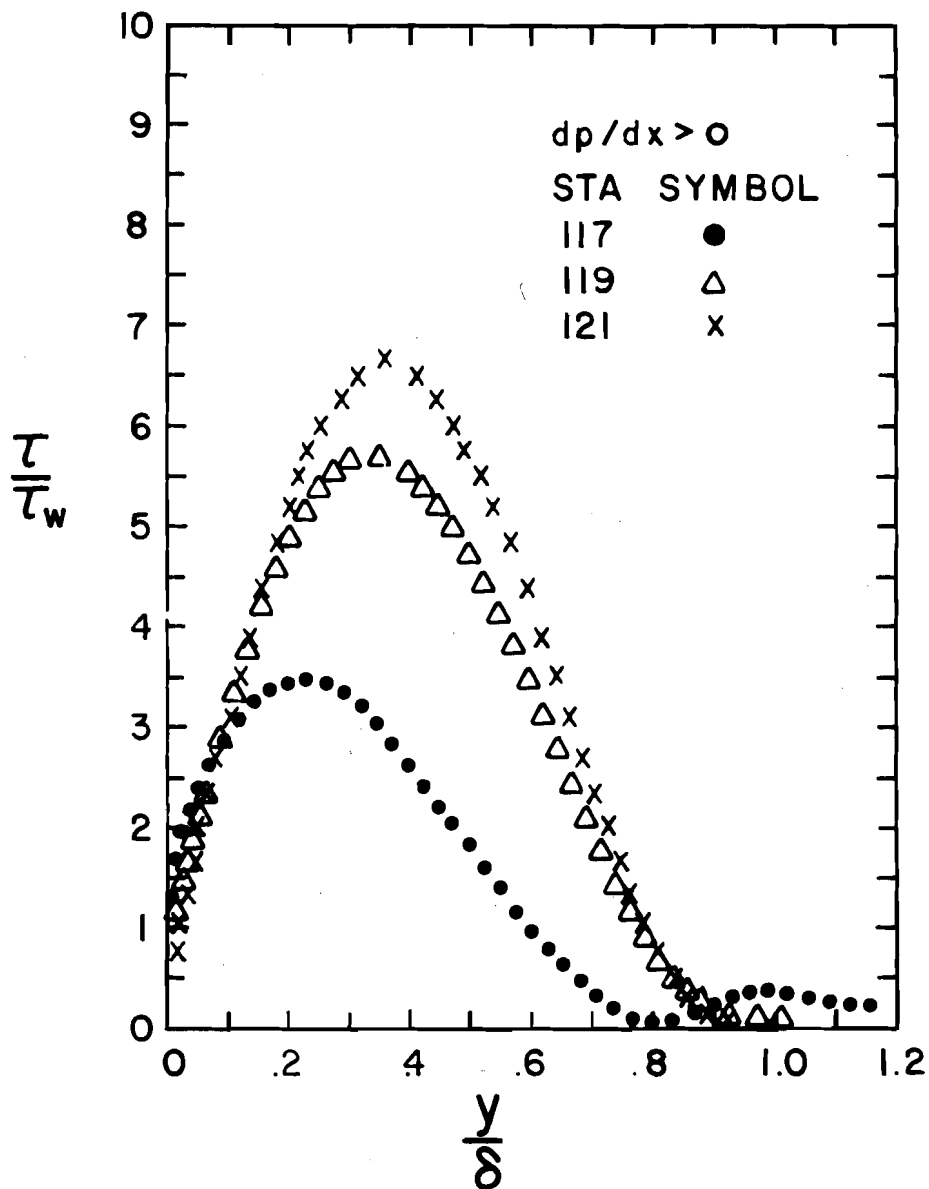


Figure 11. Calculated Shear Stress Profiles for the Flow Over the Ramp Model

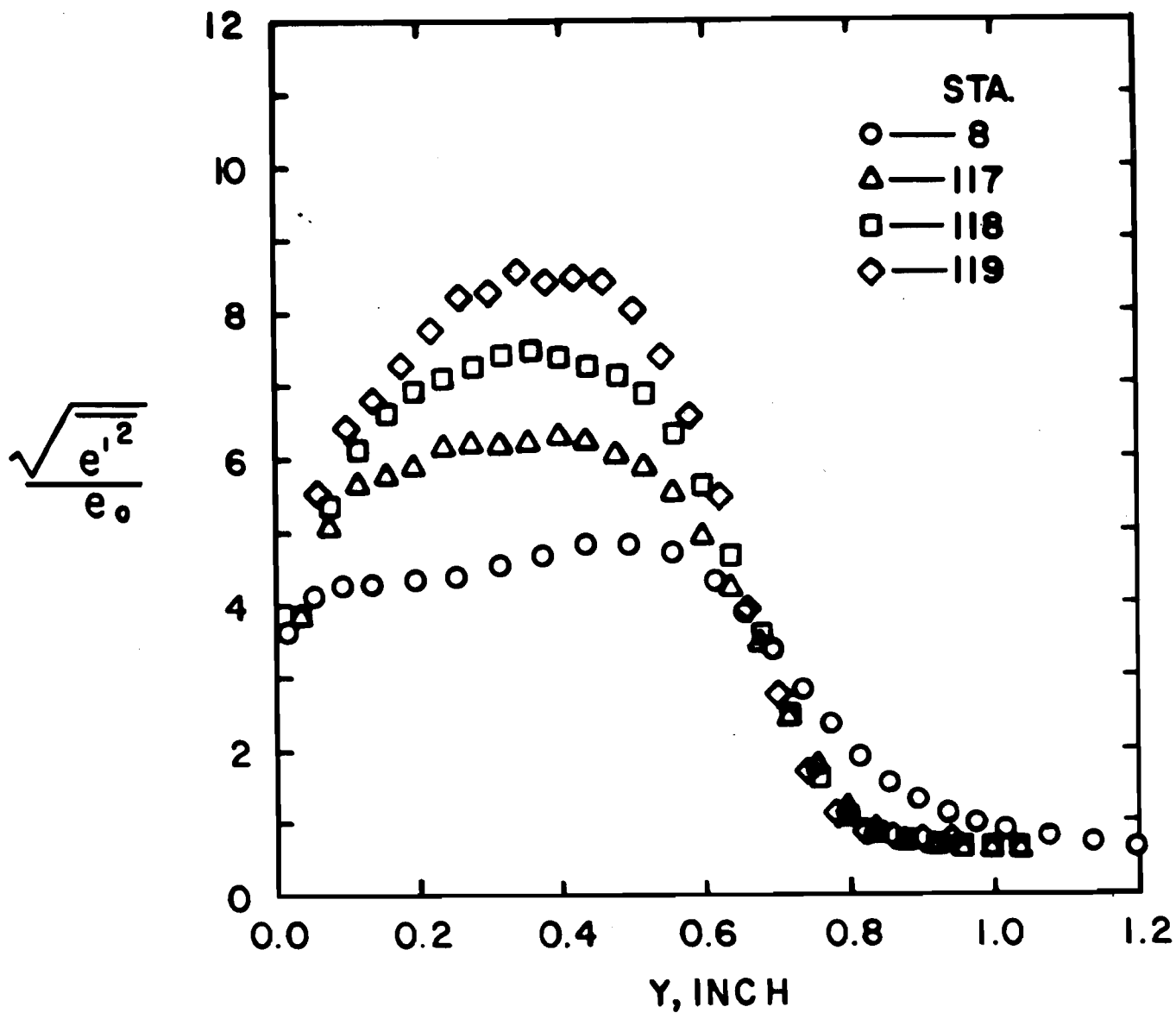


Figure 12. Turbulent Fluctuation Data Obtained Using Constant Temperature Hot Wire Anemometry

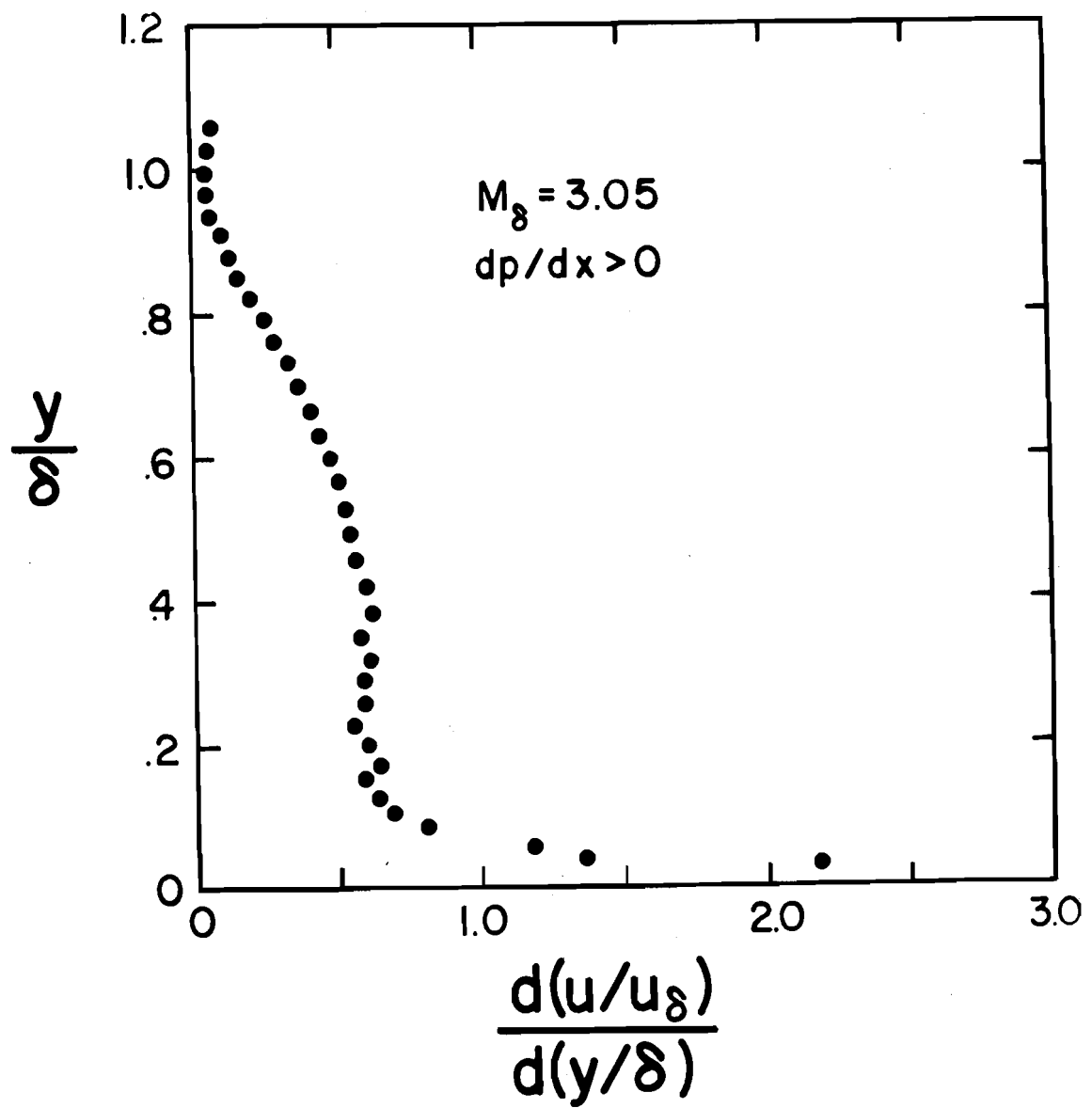


Figure 13. Velocity Derivative Profile, $dp/dx > 0$

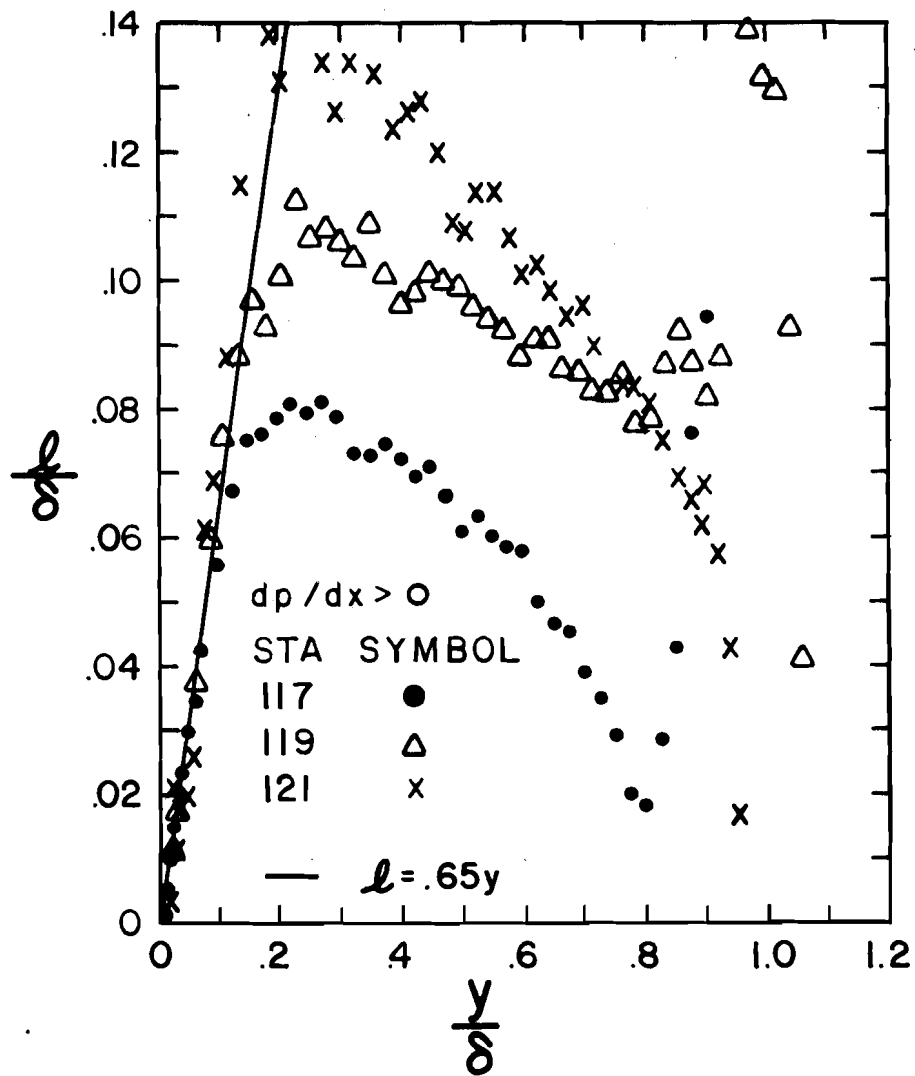


Figure 14. Calculated Mixing Length Distributions, $dp/dx > 0$

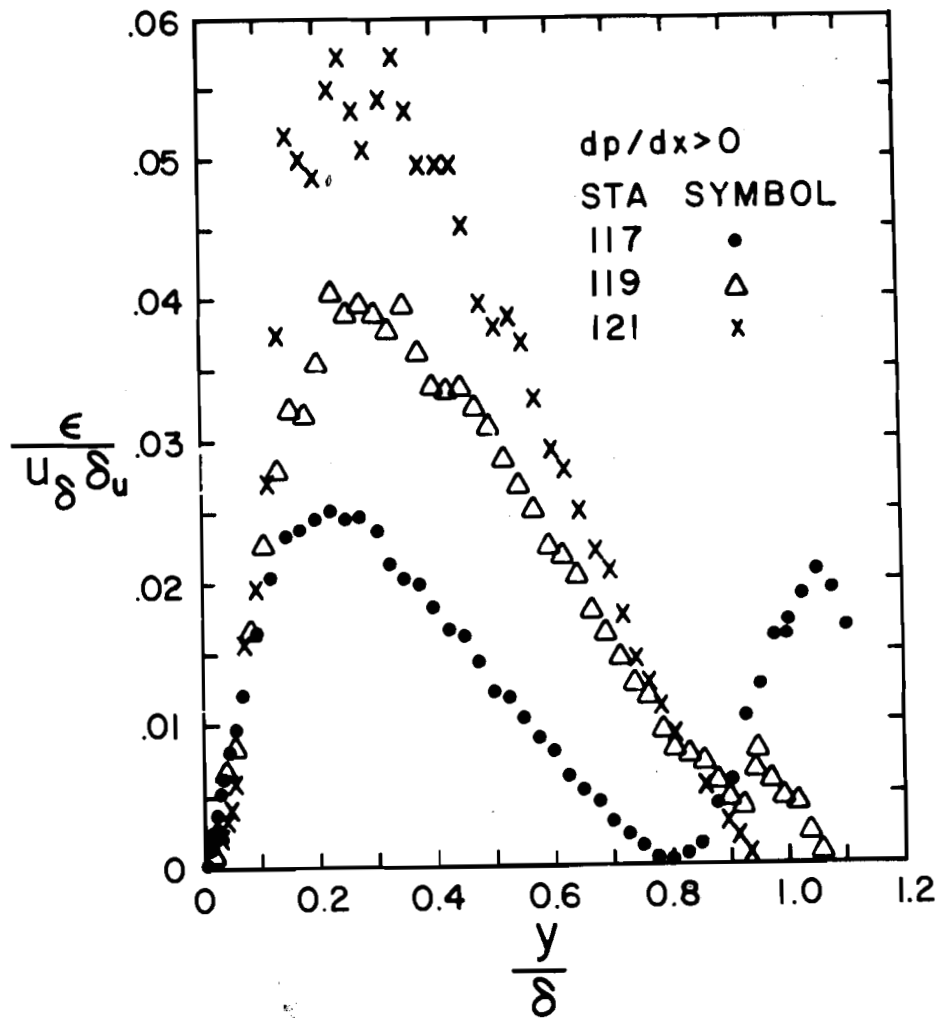


Figure 15. Calculated Eddy Viscosity Distributions, $dp/dx > 0$

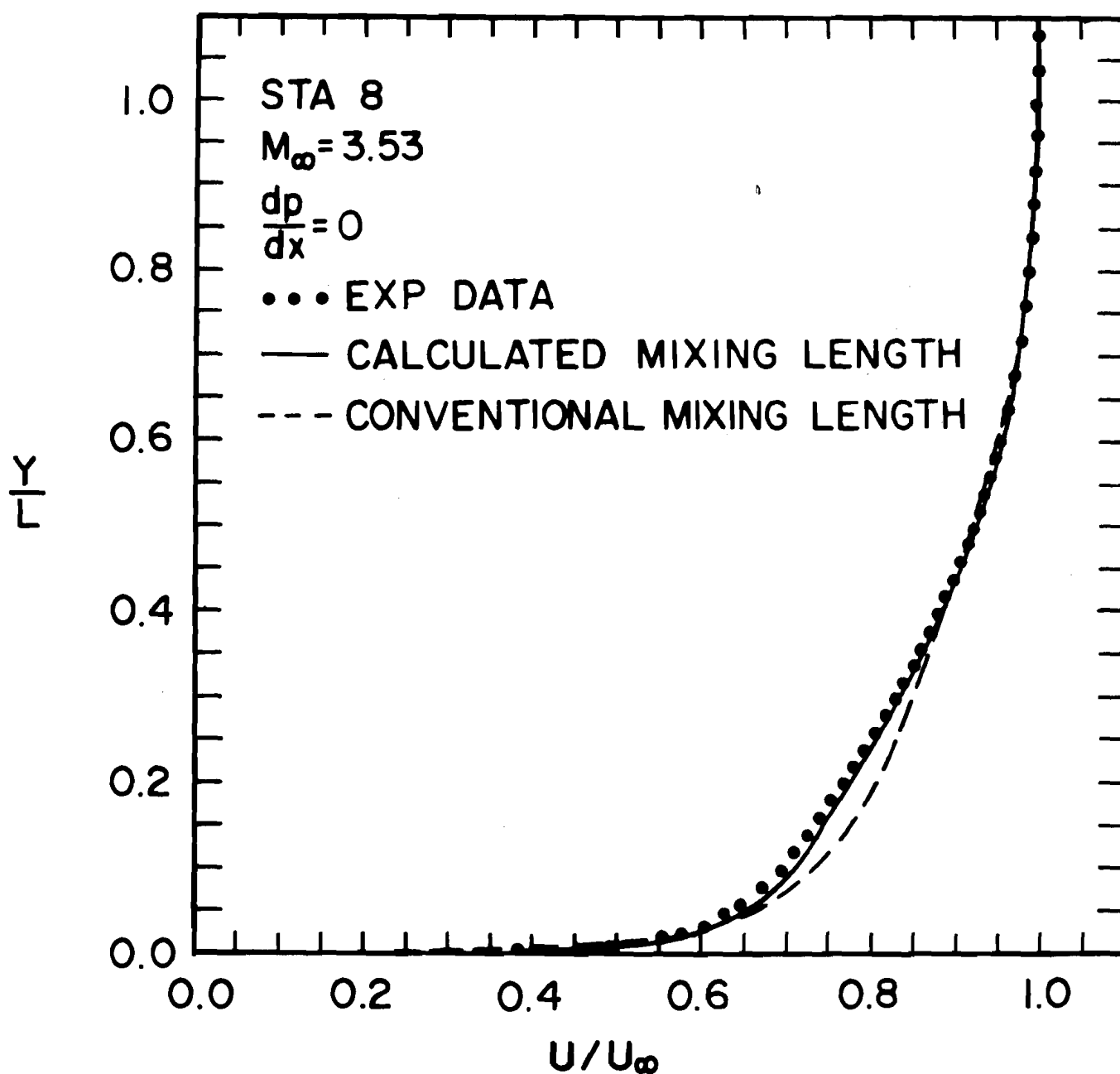


Figure 16. Comparison of Experimental Velocity Profile with Finite-Difference Computations

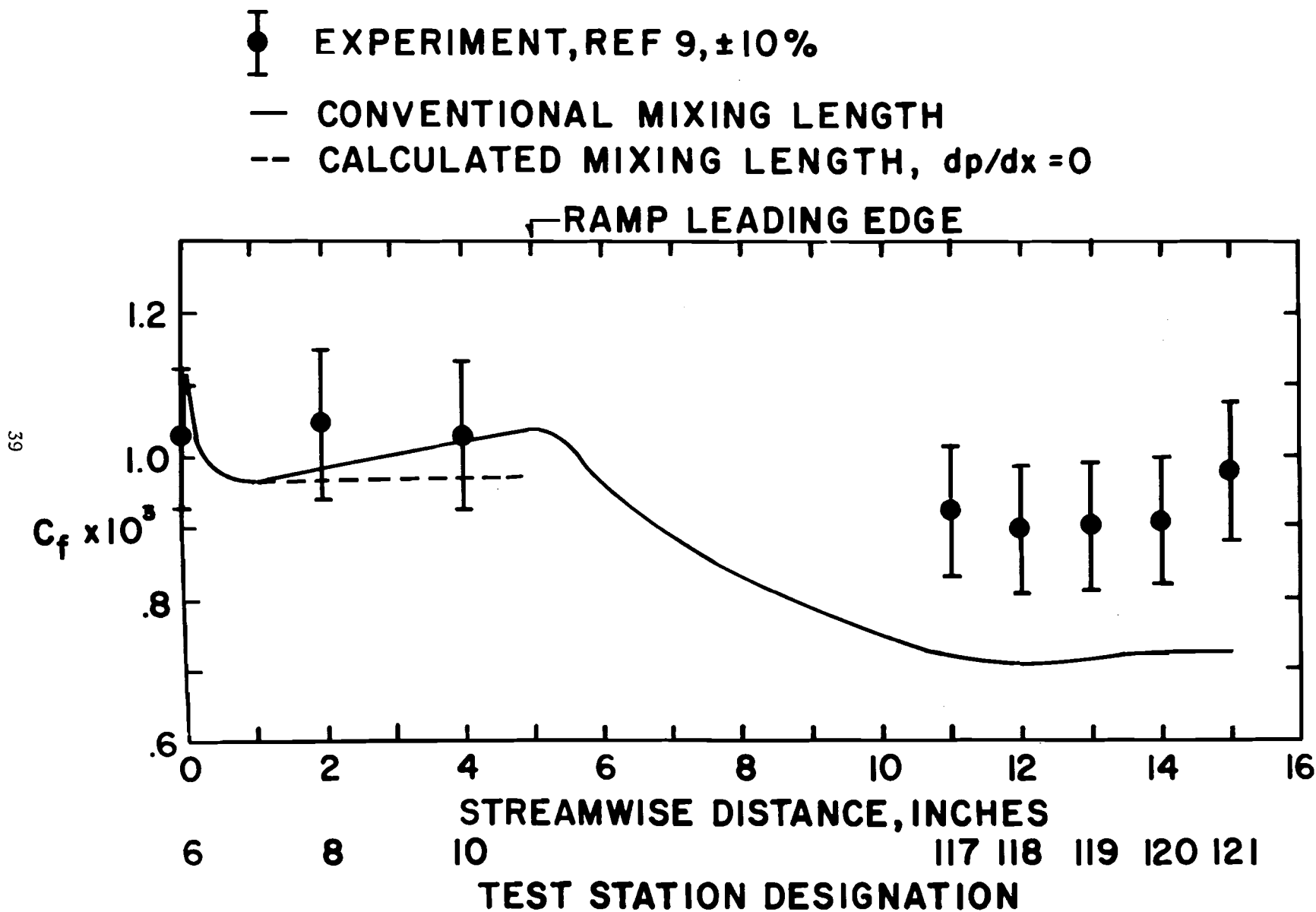


Figure 17. Numerical Calculations of Skin Friction Coefficient Compared to Experimental Measurements

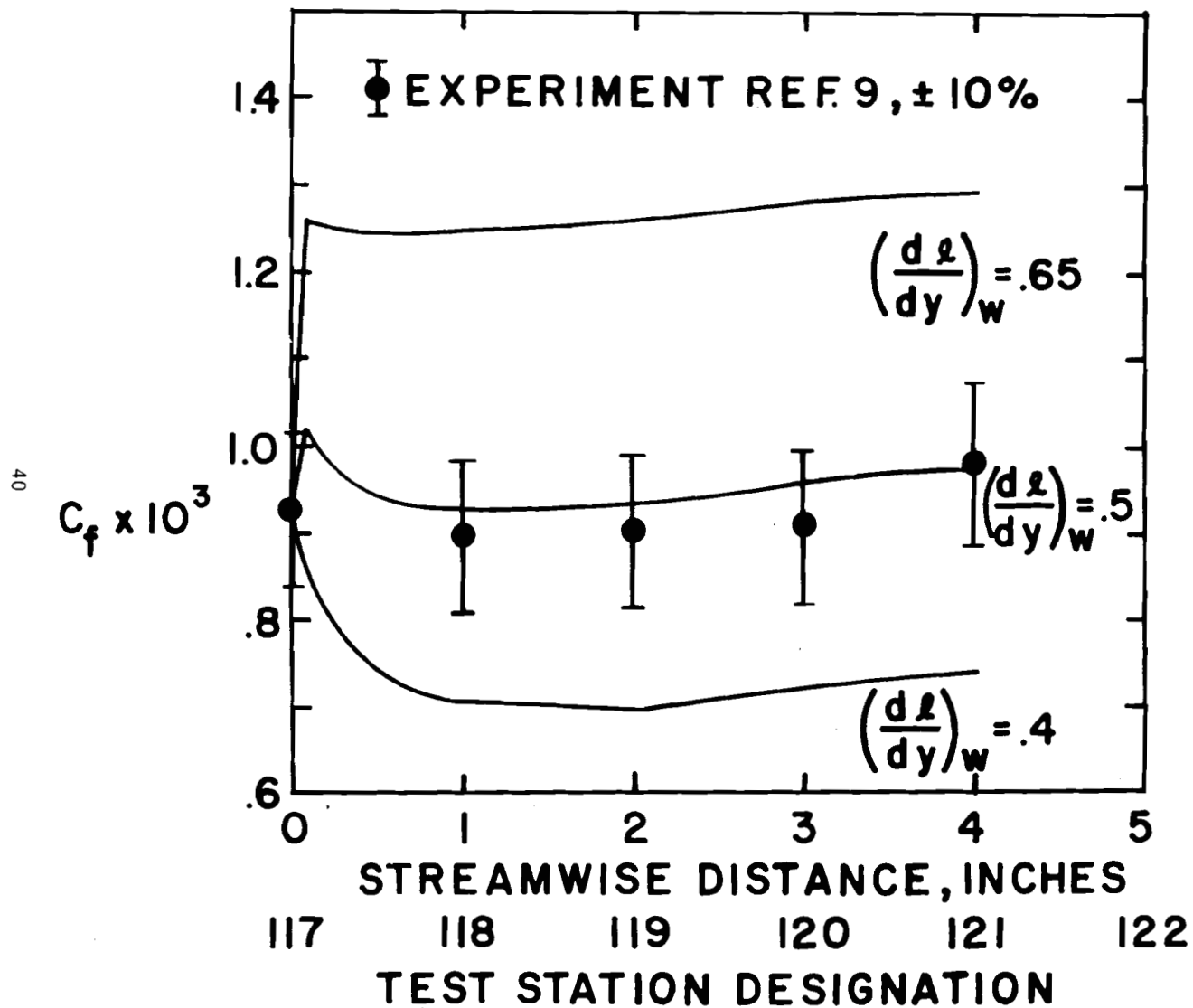


Figure 18. Comparison of Skin Friction Calculations for Adverse Pressure Gradient Flow Using Unconventional Values for K

DISTRIBUTION LIST

<u>No. of Copies</u>	<u>Organization</u>	<u>No. of Copies</u>	<u>Organization</u>
12	Commander Defense Documentation Center ATTN: TIPCR Cameron Station Alexandria, Virginia 22314	1	Commander U.S. Army Materiel Command ATTN: AMCRD-MT 5001 Eisenhower Avenue Alexandria, Virginia 22304
1	Commander U.S. Army Materiel Command ATTN: AMCDL 5001 Eisenhower Avenue Alexandria, Virginia 22304	1	Commander U.S. Army Aviation Systems Command ATTN: AMSAV-E 12th and Spruce Streets St. Louis, Missouri 63166
1	Commander U.S. Army Materiel Command ATTN: AMCDMA, MG J. R. Guthrie 5001 Eisenhower Avenue Alexandria, Virginia 22304	1	Director U.S. Army Air Mobility Research and Development Laboratory ATTN: SAVDL-D, Mr. P. Yaggy Ames Research Center Moffett Field, California 94035
1	Commander U.S. Army Materiel Command ATTN: AMCRD, MG S. C. Meyer 5001 Eisenhower Avenue Alexandria, Virginia 22304	2	Commander U.S. Army Electronics Command ATTN: AMSEL-RD AMSEL-DL Fort Monmouth, New Jersey 07703
1	Commander U.S. Army Materiel Command ATTN: AMCRD, Dr. J. V. R. Kaufman 5001 Eisenhower Avenue Alexandria, Virginia 22304	3	Commander U.S. Army Missile Command ATTN: AMSMI-R AMSMI-RDK Mr. R. Deep Mr. R. Becht Redstone Arsenal, Alabama 35809
1	Commander U.S. Army Materiel Command ATTN: AMCRD-TE 5001 Eisenhower Avenue Alexandria, Virginia 22304	1	Commander U.S. Army Tank Automotive Command ATTN: AMSTA-RHFL Warren, Michigan 48090

DISTRIBUTION LIST

<u>No. of</u> <u>Copies</u>	<u>Organization</u>	<u>No. of</u> <u>Copies</u>	<u>Organization</u>
2	Commander U.S. Army Mobility Equipment Research & Development Center ATTN: Tech Docu Cen, Bldg. 315 AMSME-RZT Fort Belvoir, Virginia 22060	1	Commander U.S. Army Natick Laboratories ATTN: AMXRE, Dr. D. Sieling Natick, Massachusetts 01762
1	Commander U.S. Army Munitions Command ATTN: AMSMU-RE Dover, New Jersey 07801	1	Commander U.S. Army Research Office (Durham) ATTN: CRD-AA-EH Box CM, Duke Station Durham, North Carolina 27706
4	Commander U.S. Army Picatinny Arsenal ATTN: SMUPA-AD Mr. S. Wasserman SMUPA-FR-S Mr. A. Loeb Mr. D. Mertz Mr. E. Falkowski Dover, New Jersey 07801	3	Commander U.S. Naval Air Systems Command ATTN: AIR-604 Washington, DC 20360
2	Commander U.S. Army Weapons Command ATTN: AMSWE-RE AMSWE-RDF Rock Island, Illinois 61202	3	Commander U.S. Naval Ordnance Systems Command ATTN: ORD-0632 ORD-035 ORD-5524 Washington, DC 20360
1	Director U.S. Army Advanced Materiel Concepts Agency 2461 Eisenhower Avenue Alexandria, Virginia 22314	1	Commander U.S. Naval Ship Research and Development Center ATTN: Dr. S. de los Santos Aerodynamics Lab Washington, DC 20007
1	Commander U.S. Army Harry Diamond Laboratories ATTN: AMXDO-TD/002 Washington, DC 20438	3	Commander U.S. Naval Ordnance Laboratory ATTN: Code 031, Mr. K. Lobb Code 312, Mr. S. Hastings Code 312, Mr. F. Ragan Silver Spring, Maryland 20910
1	Commander U.S. Army Materials and Mechanics Research Center ATTN: AMXMR-ATL Watertown, Massachusetts 02172	2	Commander U.S. Naval Weapons Laboratory ATTN: Dr. W. Kemper Mr. C. Wingo Dahlgren, Virginia 22448

DISTRIBUTION LIST

<u>No. of Copies</u>	<u>Organization</u>	<u>No. of Copies</u>	<u>Organization</u>
1	AFATL (DLR) Eglin AFB Florida 32542	1	Sandia Corporation ATTN: Div. No. 9322 Mr. W. Curry P. O. Box 5800 Albuquerque, New Mexico 87115
1	AFATL (DLRD) Eglin AFB Florida 32542	2	Massachusetts Institute of Technology ATTN: Prof. E. Covert Prof. C. Haldeman 77 Massachusetts Avenue Cambridge, Maryland 20139
1	AFATL (DLRV) Eglin AFB Florida 32542	1	University of Notre Dame Department of Aerospace Engineering ATTN: Dr. J. Nicolaidis Notre Dame, Indiana 46556
1	Director Jet Propulsion Laboratory ATTN: Mr. B. Dayman 4800 Oak Grove Drive Pasadena, California 91103	1	University of Virginia Department of Aerospace Engineering and Engineering Physics ATTN: Prof. I. Jacobson Charlottesville, Virginia 22904
1	Calspan Corporation ATTN: Mr. J. Andes, Head Transonic Tunnel Dept P. O. Box 235 Buffalo, New York 14221		
			<u>Aberdeen Proving Ground</u> Ch, Tech Lib Marine Corps Ln Ofc CDC Ln Ofc Dir, USAMSAA ATTN: Dr. J. Sperrazza

UNCLASSIFIED

Security Classification

DOCUMENT CONTROL DATA - R & D

(Security classification of title, body of abstract and indexing annotation must be entered when the overall report is classified)

1. ORIGINATING ACTIVITY (Corporate author) US Army Ballistic Research Laboratories Aberdeen Proving Ground, Maryland 21005		2a. REPORT SECURITY CLASSIFICATION UNCLASSIFIED	
3. REPORT TITLE CALCULATIONS OF TURBULENT SHEAR STRESS IN SUPERSONIC TURBULENT BOUNDARY LAYER ZERO AND ADVERSE PRESSURE GRADIENT FLOW		2b. GROUP	
4. DESCRIPTIVE NOTES (Type of report and inclusive dates)			
5. AUTHOR(S) (First name, middle initial, last name) Walter B. Sturek			
6. REPORT DATE June 1973	7a. TOTAL NO. OF PAGES 43	7b. NO. OF REFS 15	
8a. CONTRACT OR GRANT NO.	8b. ORIGINATOR'S REPORT NUMBER(S)		
8. PROJECT NO. RDT&E Project No. 1T061102A33D	BRL Report No. 1651		
c.	9b. OTHER REPORT NO(S) (Any other numbers that may be assigned this report)		
d.			
10. DISTRIBUTION STATEMENT Approved for public release; distribution unlimited.			
11. SUPPLEMENTARY NOTES		12. SPONSORING MILITARY ACTIVITY U.S. Army Materiel Command 5001 Eisenhower Avenue Alexandria, Virginia 22304	
13. ABSTRACT Calculations of turbulent shear stress distributions are reported for zero pressure gradient and adverse pressure gradient supersonic turbulent boundary layer flow. The calculations are accomplished by numerically integrating the equation for conservation of streamwise momentum using mean profile experimental data. The mixing length distributions have also been determined and indicate that the mixing length distribution is significantly altered for the adverse pressure gradient flow. Finite difference boundary layer computations using an altered mixing length distribution show improved agreement with experimental measurements of skin friction for the adverse pressure gradient flow.			

DD FORM 1473

REPLACES DD FORM 1473, 1 JAN 66, WHICH IS OBSOLETE FOR ARMY USE.

UNCLASSIFIED
Security Classification

14.	KEY WORDS	LINK A		LINK B		LINK C	
		ROLE	WT	ROLE	WT	ROLE	WT
	turbulent shear stress distribution turbulence supersonic turbulent boundary layer zero pressure gradient adverse pressure gradient finite difference calculations mean profile data						